Performance Assessment of a Dual-purpose HP-TES for a Typical Year Comparing Different Climate Zones

Al-Hussain OTHMAN[1], Vikrant AUTE[2]*, James TANCABEL[3]

[1,2,3]Center for Environmental Energy Engineering,
Department of Mechanical Engineering, University of Maryland,
College Park, MD 20742, USA
Email: [1]aothman@umd.edu, [2]vikrant@umd.edu, [3]jmtanc@umd.edu

* Corresponding Author

ABSTRACT

Complete electrification of heating and cooling systems in the United States would overload the existing electrical grid. To this end, recent research efforts have focused on energy storage as one way to reduce ever-increasing peak electricity demands. One such technology is heat pump integrated thermal-energy storage (HP-TES) systems, which can enable load-shifting and reduce demand during peak hours. In this work, a Modelica model of a 4-Ton, dual-mode (heating and cooling) HP-TES system using a room-temperature phase-change material (PCM) integrated through a secondary hydronic loop was developed and simulated for a typical meteorological year in Riverside, CA (ASHRAE Climate Zone 2B), and Chicago, IL (ASHRAE Climate Zone 5A), for a DOE small office prototype building. The COP improvement and demand reduction were analyzed during the time-of-use peak hours along with the required recharge cycle energy demand. A typical summer in Riverside, CA resulted in model-predicted peak COP increases of 50 – 100% compared to the baseline heat pump, especially at higher outdoor temperatures, coupled with maximum peak energy reductions of 22%. During shoulder and winter season simulations, heating energy savings were higher as outdoor temperatures dropped below the PCM phase change temperature. For Chicago, IL, backup heating was necessary to meet the required system capacity for very cold ambient conditions, resulting in winter peak energy savings between 16 – 60% when accounting for backup heating requirements. The recharge energy was found to be mostly below the baseline HP energy during the peak. With improved component selections and controls, the recharge energy may be reduced. The outcomes from the simulations can provide first-order estimates for potential peak energy savings, challenges, and required controls in any location before conducting any field testing.

1. INTRODUCTION

Current efforts to reduce CO_2 emissions by electrifying heating and cooling systems across the United States will overly strain the present-day electrical grid, especially during peak hours (US Dept. of Energy, 2024). Thus, substantial research efforts are investigating integrated sensible and latent thermal energy storage (TES) systems with heat pumps (HPs) to shift and reduce peak electrical loads. In many integrated HP-TES system examples (Arteconi et al., 2013; D'Ettorre et al., 2019; Fischer et al., 2014), the thermal energy storage serves as the heat sink/source to cool/heat the indoor space during peak time-of-use hours.

TES can be integrated with HPs in many forms. Said & Hassan (2018) experimentally pre-cooled the outdoor air before condenser entry using air-side latent phase-change material (PCM) panels, reducing power consumption by almost 12% at 45°C outdoor temperatures. Huang et al. (2020) conducted theoretical studies and field tests for solar thermal collectors coupled with ground-source HPs and hot water sensible TES tanks in a Chinese village, reducing water heating energy consumption by 70% along with COP increases of around 10%. The ability of integrated HP-TES to achieve certain economic and energy performance metrics depends on the system, location, and control strategy. Ermel et al. (2023) simulated a hot water TES tank in Denver, CO, used to heat the radiator when the ambient temperature was less than 7°C, while the HP operates for the rest of the day. While heating capacity improvement was observed, almost no economic savings were observed due to the use of a flat utility rate. On the other hand, Shi et al. (2021) estimated a potential 18% reduction in peak demand in all US single-family homes for a combined ground-source HP with an underground water-PCM TES tank.

In this paper, we investigate the performance of a 4-ton (14.1 kW) dual-purpose HP-TES for an entire year in two ASHRAE US climate zones (CZs), namely US CZ 2B (Riverside, CA) and US CZ 5A (Chicago, IL). The latent TES system utilizes a 22°C salt-hydrate PCM, which is used as a heat source in heating mode, and a heat sink in cooling mode. Transient models of the HP and HP-TES were developed in Modelica and simulated for a typical meteorological year for the DOE prototype small office building boundary conditions using Spawn of EnergyPlus™ (EnergyPlus™, 2017; Wetter et al. 2014). HP-TES system insights and challenges are discussed in detail.

2. METHODOLOGY

2.1 System Description

The proposed HP-TES system is a 4-ton (14.1 kW) heating and cooling air-source R410A system with a 22°C PCM thermal battery. The room-temperature thermal battery is integrated into the cycle using a secondary hydronic loop containing a plate heat exchanger (PHX) and single-speed pump. During discharge operation (Figure 1(a)), the thermal battery becomes the lower temperature heat sink in cooling mode / higher temperature heat source in heating mode, replacing the outdoor unit. During recharge modes (Figure 1(b)), the operations are reversed and the indoor coil is disconnected to solidify the PCM for future cooling mode operation / melt the PCM for future heating mode operation.

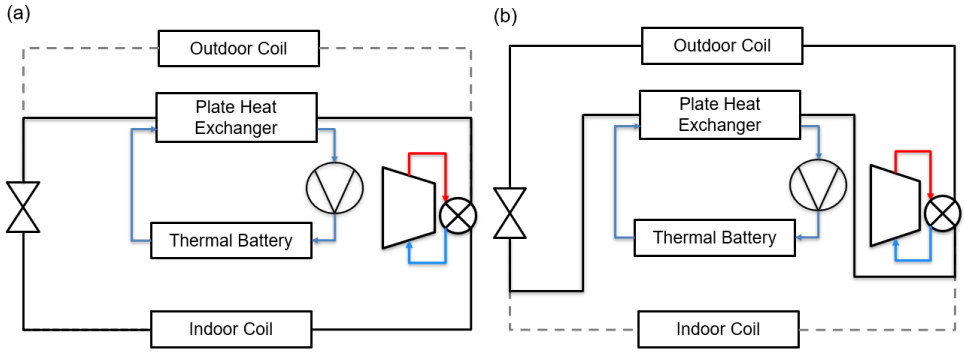

Figure 1: HP-TES integrated system: (a) discharge mode; (b) recharge mode.

2.2 Thermal Battery Sizing

The thermal battery was sized to meet the required storage capacity and discharge rate in cooling mode assuming a COP of 3.5, as cooling has the highest capacity required (18 kW). The thermal battery was sized to meet the required system capacity for two hours (Equation (1)).

$$V_{PCM} = \frac{\int_0^{2hr} \dot{Q} dt}{\rho_{PCM} \cdot H_{sl}} \tag{1}$$

A salt-hydrate PCM was used for its higher thermal conductivities compared to organic PCMs (Hirschey et al., 2018), and has a nominal enthalpy of fusion of 190 kJ/kg and a nominal density of 1500 kg/m^3. The heat exchanger size required to meet the discharge rate of 18 kW was determined by Equation (2). The LMTD was calculated using the PCM glide of 4.5 K and the secondary fluid temperature change. The required secondary fluid and PCM surface areas were then calculated, and a commercial tube-fin HX was selected to meet the surface area requirement.

$$UA_{req} = \frac{\dot{Q}_{dis}}{LMTD} \qquad A_{PCM,req} = \frac{1}{h_{PCM}} \left[\frac{1}{UA} - \frac{1}{(hA)_{HTF}} \right]^{-1} \tag{2}$$

2.3 Heat Pump Component & System Modeling

The baseline and HP-TES components were modeled using an in-house Modelica Library (Qiao et al., 2015). The indoor and outdoor units are microchannel heat exchangers (MCHXs) that consist of finite segmented refrigerant and air-side control volumes (CVs), connected by a wall CV (Figure 2). In this model, axial conduction is neglected, and

the heat transfer is directly to and from the refrigerant and air. The refrigerant CV solves the transient conservations of mass and energy. The Shah (2017) correlation was used to compute the evaporation two-phase heat transfer coefficient, while the Shah (2019) correlation was used for refrigerant two-phase condensation. The Dittus & Boelter, (1930) correlation was used to compute the single-phase heat transfer coefficients in both HX.

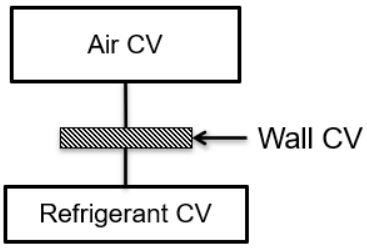

Figure 2: MCHX model control volume representation in Modelica.

The air control volume computes the sensible and latent heat transfer considering the fin efficiencies and corrects the heat transfer coefficient using the Lewis analogy (Dhumane et al. 2018; Hong & Webb, 1996). The Chang & Wang, (1997) correlation was used to estimate the air-side heat transfer coefficient. The wall control volume accounts for the heat transfer across the tube wall as shown in Equation (3), where $\dot{Q}_r$ and $\dot{Q}_a$ are conduction heat transfers from one side of the tube wall to the other. More details about the MCHX can be found at Dhumane et al., (2021) and Qiao et al., (2015).

$$(m_{tube}c_{tube} + m_{fins}c_{fins})\frac{dT_{tube}}{dt} = \dot{Q}_r + \dot{Q}_a \tag{3}$$

This system uses a single-speed scroll compressor that was modeled using the manufacturer-specified 10-coefficient compressor map (AHRI Standard 540, 2020), and adjusted using the Dabiri & Rice, (1981) correction factor. The electronic expansion valve was modeled using Equation (4) where the orifice opening was adjusted using a PI controller based on the suction superheat that was set to 5 K.

$$\dot{m}_{exp} = \frac{u}{u_{max}} C_v A\sqrt{\rho_{in}\Delta P} \tag{4}$$

The secondary hydronic loop components are the plate heat exchanger (PHX), single-speed pump, and thermal battery. The representation of the secondary loop component models in Modelica is shown in Figure 3. The PHX model combined all the plates and channels and consisted of the same refrigerant and wall CV used in the MCHXs and a water control volume. For the refrigerant control volume, Focke et al. (1985) correlation was used for the single-phase heat transfer coefficient, and Yan et al. (1999) correlation was used for the two-phase heat transfer coefficient. The water control volume calculated the heat transfer using Equation (5).

$$\dot{Q}_{total} = \sum_{j=1}^{j=N_{seg}} h_{seg,j} A_{seg,j} (T_{wall,j} - T_{water,j-1}) \tag{5}$$

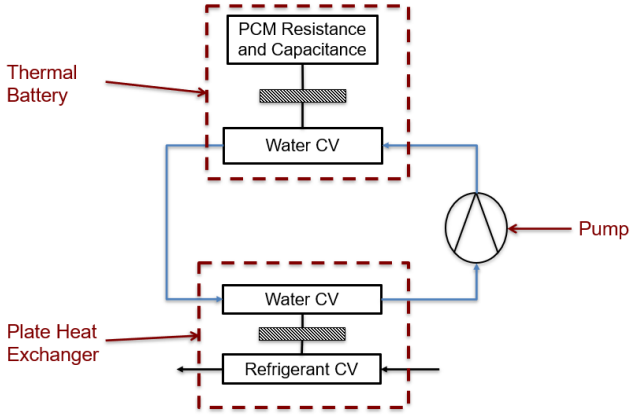

Figure 3: Representative schematic of the secondary loop components in Modelica.

The thermal battery consists of the same water CV at the PHX represented in Equation (5), where the water heat transfer coefficient is obtained from the Dittus & Boelter, (1930) correlation. The PCM was modeled by a resistance-capacitance model. The capacitance was modeled using manufacturer-provided DSC curves. The energy release rate was computed using Equation (6), where *i* is the enthalpy and *M* is the PCM mass.

$$\dot{Q} = \sum_{j=1}^{j=N_{seg}} \frac{di_{PCM,j}}{dt} M_{PCM,j} \tag{6}$$

The resistance component of the thermal battery computes the heat flow rate from the PCM to the tube wall using PCM thermal conductivity *k* and half the equivalent distance *L* between HX tubes, shown in Equation (7).

$$\begin{aligned} \dot{Q}_{PCM} &= \frac{k}{L} \sum_{j=1}^{j=N_{seg}} A_{seg,j} (T_{wall,j} - T_{water,j-1}) \\ L &= \frac{\sqrt{(VS - OD)^2 + (HS - OD)^2}}{2} \end{aligned} \tag{7}$$

The single-speed pump power was calculated assuming a pump efficiency of 70%, and the mass flow rate was fixed to maintain a temperature change of 5 K in the secondary loop (Equation (8)).

$$\dot{W}_{pump} = \frac{\dot{m}\Delta P}{\rho \eta} \tag{8}$$

Finally, all vapor-compression cycle and secondary loop components were connected using `FluidPorts` and `HeatPorts` for fluid flow and heat transfer, respectively, using the `Modelica Standard Library (2013)`.

2.4 System Operation

The HP-TES was sized to provide 4-tons (14.1 kW) of cooling or heating for 2 hours. The peak hours in each location were selected as per their utility providers (Table 1). The discharge hours were chosen based on achieving the maximum demand reduction when switching from HP to HP-TES within the utility peak hours. As Riverside, CA, is a cooling-dominated region, it makes more sense to operate the TES when it is the warmest during peak hours. The opposite operation was used in Chicago, IL, where the TES was utilized during the coolest hours of the super-peak and peak periods to maximize cost savings and lower temperature lifts. The recharge hours were selected during nighttime when the building was unoccupied at the lowest energy cost with the minimum temperature lift. The recharge cycle is considered "complete" when the PCM completely changes phase from solid to liquid or vice versa.

Table 1: Utility peak hours, HP-TES discharge, & recharge times for Riverside, CA, & Chicago, IL

ASHRAE Climate Zone	Location	Utility Peak Hours	Discharge Hours	Recharge Hours
2B	Riverside, CA	4 – 9 PM (SCE, 2023)	Cooling: 4 – 6 PM Heating: 6 – 8 PM	2 – 5 AM
5A	Chicago, IL	Super Peak: 2 – 7 PM Peak: 6 AM – 2 PM 7 – 10 PM (ComEd, 2024)	Cooling: 2 – 4 PM Heating: 6 – 8 PM	Cooling: 2 – 5 AM Heating: 10 PM – 2 AM

For the remaining hours of the day, the baseline HP system is on or off depending on the building's operating hours. The building simulated using the Spawn of EnergyPlus™ (EnergyPlus™, 2017; Wetter et al., 2014) was the small-office prototype building (Dept. of Energy Building Technologies Office, 2022) operating from 6 AM to 8 PM every day. The HP-TES indoor boundary conditions were obtained from pre-coil air conditions obtained from Spawn. The outdoor boundary conditions were obtained from TMY3 data for both locations (Wilcox & Marion, 2008).

3. RESULTS AND DISCUSSION

3.1 Riverside, CA (ASHRAE Climate Zone 2B)

To assess the system potential in Riverside, CA, the baseline HP and HP-TES simulated performances were compared at peak hours. Figure 4 shows the COP improvements for the HP-TES in cooling (discharge) mode compared with baseline HP operating at different outdoor temperatures in July. As the HP-TES disconnects the cooling cycle from the outdoor HX, the heat sink temperature drops, considerably reducing the temperature and pressure lifts and increasing the COP. This is most effective when the outdoor temperatures are significantly higher than PCM temperatures, resulting in maximum savings in extreme ambient conditions. The profile of the HP-TES curves in Figure 4 changes from a steep-to-gentle slope during melting as the PCM transitions from sensible heating in the solidus state to two-phase melting. Although the COP decreases from 6.5 to 4.5 as the PCM melts, this performance is still 50% higher than the baseline HP operation when the outdoor temperature is 35°C.

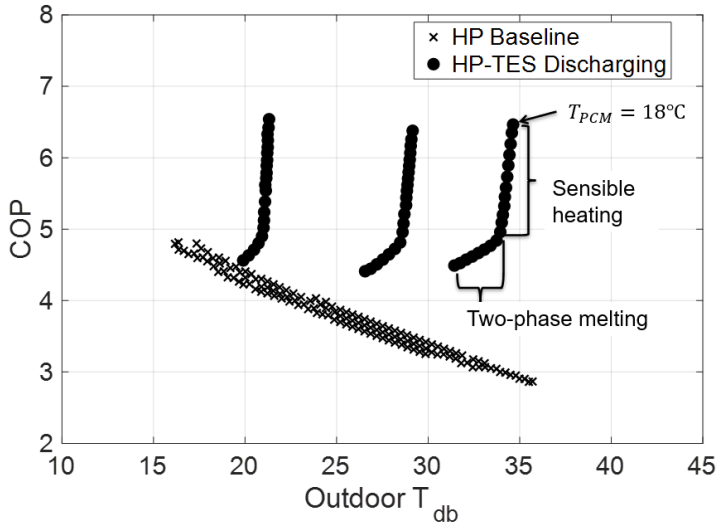

Figure 4: Simulated performance of the baseline HP and HP-TES in July (Wilcox & Marion, 2008) for Riverside, CA.

As the winter and shoulder seasons in Riverside, CA, are still somewhat warm, the system was simulated in both cooling and heating to find the highest COP increases. Looking at the simulated performance in February for both heating (Figure 5(a)) and cooling modes (Figure 5(b)), there is more potential to use the HP-TES system in heating

mode given the higher COP throughout the discharge process. This is due to the PCM melting temperature being higher than the outdoor temperature during the peak.

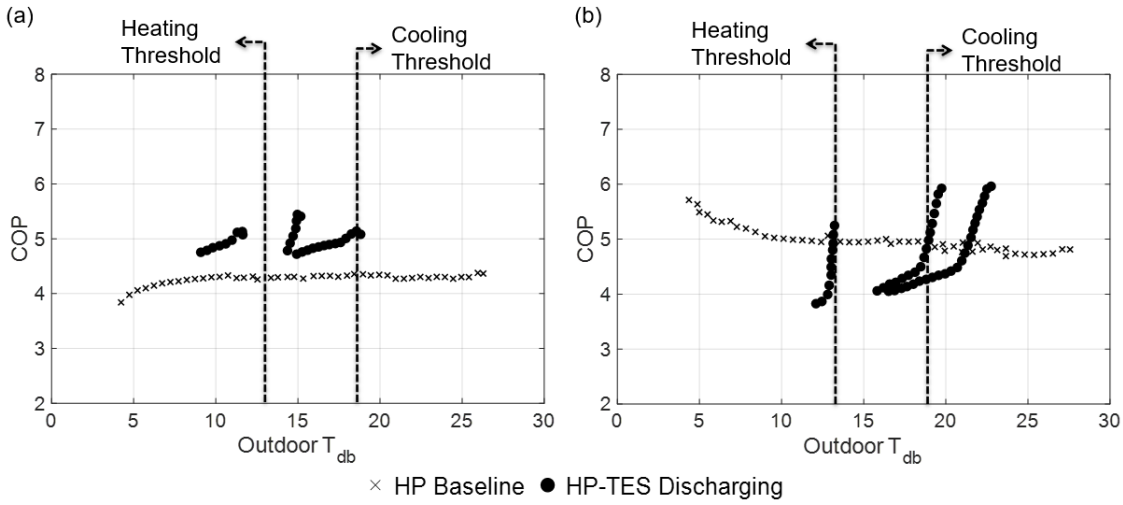

Figure 5: Simulated performance of the baseline HP and HP-TES for February (Wilcox & Marion, 2008) for Riverside, CA in (a) heating, and (b) cooling modes.

The energy required by the baseline HP and the HP-TES during the peaks was assessed for cooling and heating modes (Figure 6). The peak energy savings were assessed in cooling mode in the summer months (June-September), while the savings for both cooling and heating modes were evaluated for the rest of the year. During summer, the HP-TES can reduce energy consumption during peak hours by 15 – 22%. Although the maximum temperature happens in September, the highest peak energy savings occur in July, as the peak temperature hours and peak utility hours overlap in July but not September. During the shoulder and winter months, cooling mode HP-TES showed no potential energy savings during the peak as the outdoor temperatures are higher than the PCM melting temperature. On the other hand, the peak energy savings in heating mode for the shoulder and winter months are 7 – 15%, with the lowest savings occurring in February, and the highest savings in December, again directly correlating to ambient temperatures during peak operation.

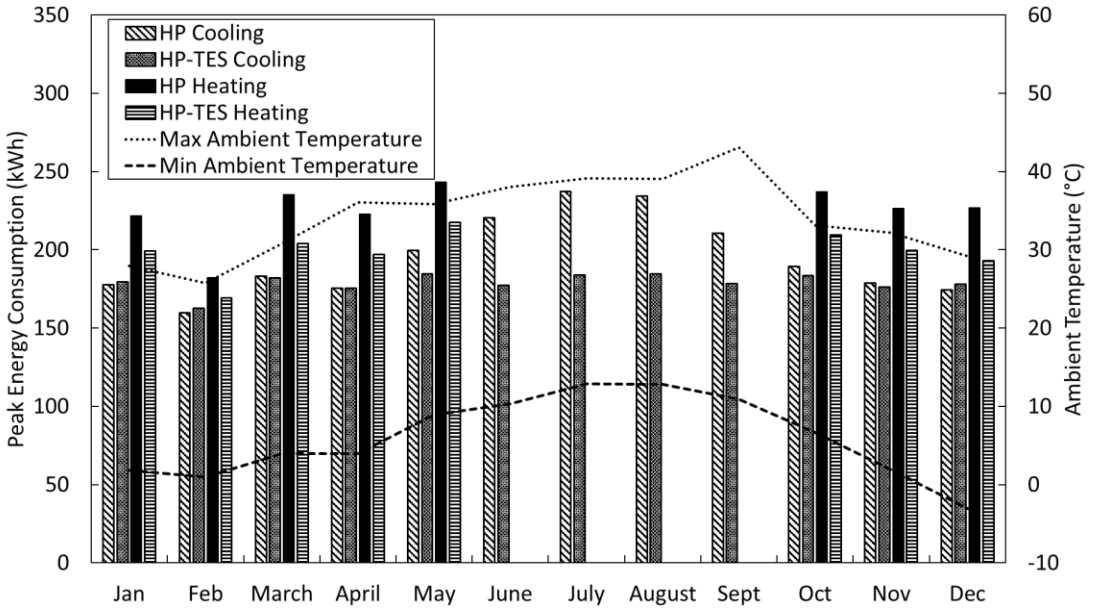

Figure 6: Cumulative monthly energy consumption during the peak hours in Riverside, CA.

The recharge energy was compared with the baseline and HP-TES discharge energy to assess the grid impact during nighttime hours (Figure 7). Ideally, the recharge energy should be lower than the shifted energy to achieve energy savings, while cost savings rely on the peak and off-peak utility rates. Nonetheless, to ensure that the grid is not strained at nighttime, the energy required to recharge the TES should be below the baseline HP energy consumption during the peak hours. It was found that the recharge energy was lower than discharge energy during winter and shoulder seasons, suggesting that additional component and control improvements are required to minimize recharge energy demand, especially during the summer months to (i) increase economic savings and (ii) achieve energy savings.

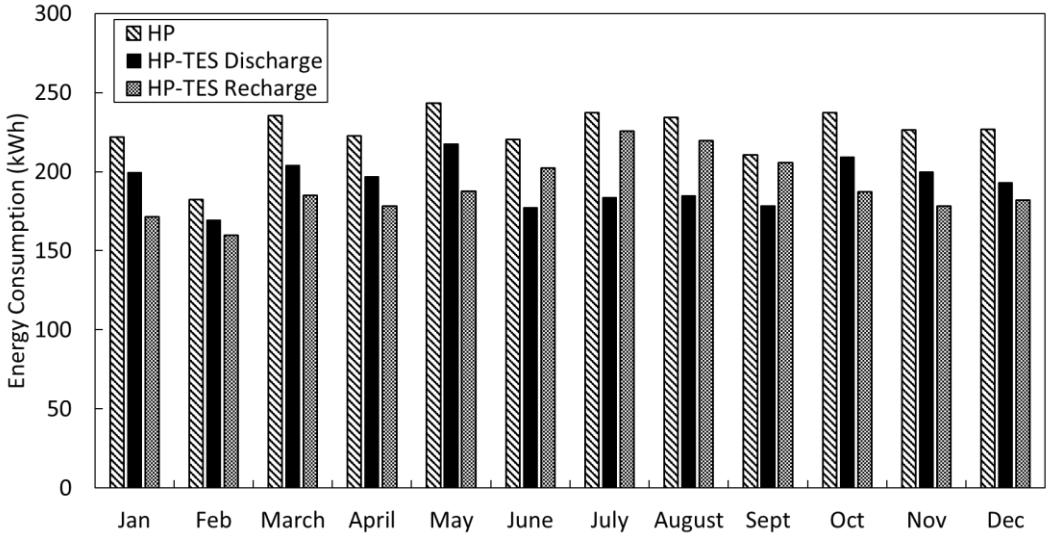

Figure 7: Comparison of peak monthly discharge and recharge energy consumption for the HP and HP-TES

3.2 Chicago, IL (ASHRAE Climate Zone 5A)

The COP improvement in cold climate conditions was at least by a factor of 2 – 3 (Figure 8(a)) and was primarily due to the increase in total heating capacity for the baseline HP (7 kW at -10°C) compared to the HP-TES (15 – 17 kW) (Figure 8(b)). This is due to the reduced temperature lift, i.e., the system evaporating temperature is considerably increased during HP-TES operation. Thus, the HP-TES system will eliminate the need for backup heating during peak hours, providing substantial peak energy savings in very cold ambient conditions. The summer months of June to August resemble a similar behavior as the summer months of Riverside, CA, e.g., May and September show the potential of using the HP-TES in both heating and cooling modes depending on the outdoor ambient temperature. Overall monthly energy consumption can help guide the operating strategy to maximize energy and economic savings.

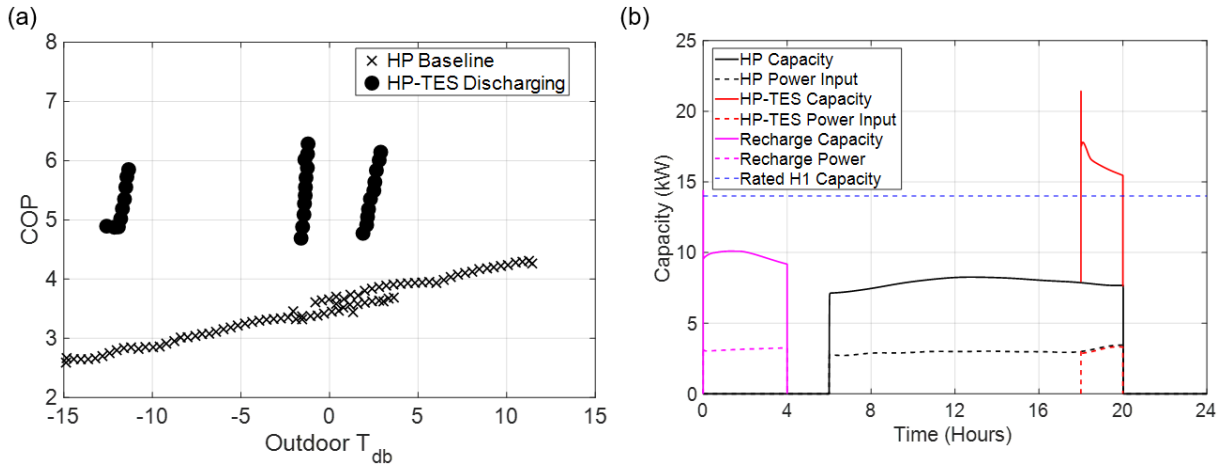

Figure 8: (a) Simulated performance for the baseline HP and HP-TES for January (Wilcox & Marion, 2008) in Chicago, IL; (b) Operation for TMY3 January 10th in Chicago, IL

When assessing the peak energy savings in heating mode (Figure 9) with the backup heating (COP = 1) to meet the system capacity, the peak demand reduction ranges from 15.8% in September to 59% in January, depending on the heating degree days required per month. These savings directly correspond to the elimination of backup heating during peak hours. For the summer months, the savings were 7% (September) to 18% (June), with more peak energy savings occurring in heating mode in September given the cooler peak hours.

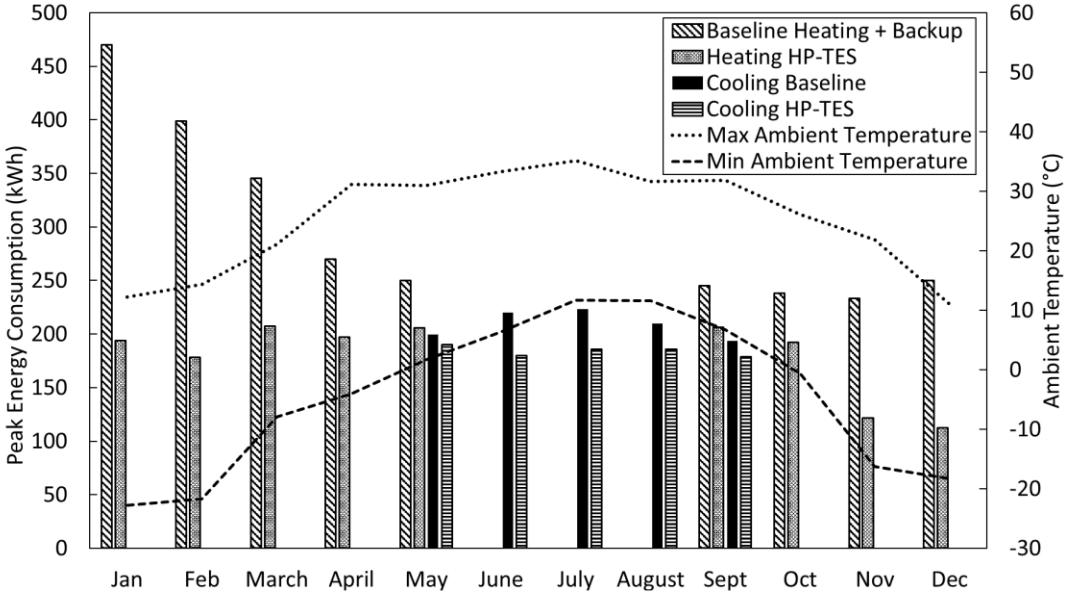

Figure 9: Cumulative monthly energy consumption during the peak hours in Chicago, IL

Investigating the recharge energy required (Figure 10) shows that for most of the year, the recharge energy is lower than the baseline but higher than the discharge energy. Except for December, the recharge energy in the winter and shoulder seasons was lower, as the baseline HP requires backup heating, increasing the peak energy demand. In December, the outdoor temperatures were so low that the recharging time increased significantly, increasing the total energy input. This further emphasizes the importance of investigating means of reducing the recharge energy. For example, May and September require both cooling and heating and daily operational controls can be implemented to recharge / discharge using the building thermal loads at different times of the day.

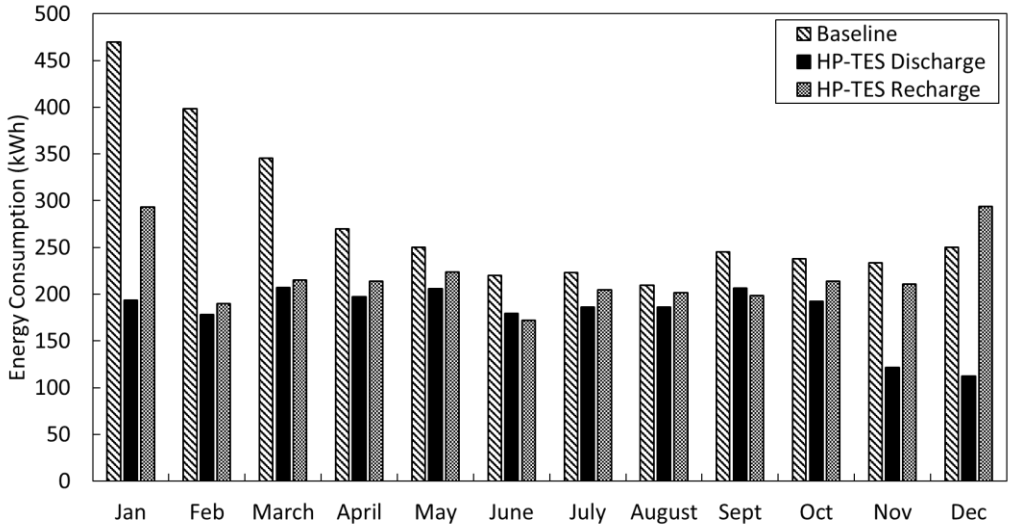

Figure 10: Comparison of peak monthly energy consumption for the baseline HP (with backup heating) and HP-TES discharge mode, with the recharge energy

6. CONCLUSIONS

In this work, a dual-purpose HP-TES system was proposed and modeled for ASHRAE Climate Zones 2B (Riverside, CA) and 5A (Chicago, IL) to identify the potential peak energy savings and challenges using off-the-shelf components. Simulation results for Riverside, CA, show that the peak cooling COP improvement was between 50 – 100% depending on the PCM state of charge at higher outdoor temperatures. The corresponding peak energy savings was between 15 – 22% depending on the ambient conditions. During the shoulder and winter seasons, heating savings were higher as outdoor temperatures were below the PCM melting temperature. For Chicago, IL, it was important to consider backup heating requirements, as the standalone HP alone cannot provide the required capacity in cold climate conditions. The HP-TES heating mode energy savings were primarily due to eliminating the need for backup heating during peak hours. For both locations, the recharge energy was lower than the baseline energy during the peak except for December in Chicago, IL. The outcomes from the simulations can provide first-order estimates for potential peak energy savings and required controls in any location before conducting any field testing.

NOMENCLATURE

A	Area	(m^2)	$\dot{Q}$	Heat transfer	(kW)
COP	Coefficient of performance	(–)	T	Temperature	(°C)
h	Heat transfer coefficient	($W \cdot m^{-2} \cdot K^{-1}$)	t	Time	(s)
HS	Horizontal spacing	(m)	VS	Vertical spacing	(m)
i	Enthalpy	($kJ \cdot kg^{-1}$)	$\dot{W}$	Power	(kW)
k	Thermal conductivity	($W \cdot m^{-1} \cdot K^{-1}$)	ΔP	Pressure drops	(Pa)
M	Mass	(kg)	η	Pump efficiency	(–)
$\dot{m}$	Mass flow rate	($kg \cdot s^{-1}$)	ρ	Density	($kg \cdot m^{-3}$)

Subscript

Comp	Compressor	Exp	Expansion Valve
db	Dry bulb	PCM	Phase change material

REFERENCES

AHRI Standard 540. (2020). *AHRI 540 (SI/ I-P): Performance Rating of Positive Displacement Refrigerant Compressors and Compressor Units | AHRI*. https://www.ahrinet.org/search-standards/ahri-540-si-i-p-performance-rating-positive-displacement-refrigerant-compressors-and-compressor

Arteconi, A., Hewitt, N. J., & Polonara, F. (2013). Domestic demand-side management (DSM): Role of heat pumps and thermal energy storage (TES) systems. *Applied Thermal Engineering*, *51*(1), 155–165. https://doi.org/10.1016/j.applthermaleng.2012.09.023

Chang, Y.-J., & Wang, C.-C. (1997). A generalized heat transfer correlation for Iouver fin geometry. *International Journal of Heat and Mass Transfer*, *40*(3), 533–544. https://doi.org/10.1016/0017-9310(96)00116-0

ComEd. (2024). *Time-of-Day Pricing | ComEd—An Exelon Company*. https://www.comed.com/ways-to-save/for-your-home/manage-my-energy/time-of-day-pricing

Dabiri, A. E., & Rice, C. K. (1981). *Compressor-simulation model with corrections for the level of suction gas superheat* (CONF-810657-2). Oak Ridge National Lab., TN (USA); Science Applications, Inc., La Jolla, CA (USA). https://www.osti.gov/biblio/6345140

Dept. of Energy Building Technologies Office. (2022). *Prototype Building Models | Building Energy Codes Program*. https://www.energycodes.gov/prototype-building-models

D'Ettorre, F., Conti, P., Schito, E., & Testi, D. (2019). Model predictive control of a hybrid heat pump system and impact of the prediction horizon on cost-saving potential and optimal storage capacity. *Applied Thermal Engineering*, *148*, 524–535. https://doi.org/10.1016/j.applthermaleng.2018.11.063

Dhumane, R., Ling, J., Aute, V., & Radermacher, R. (2021). Performance comparison of low GWP refrigerants for a miniature vapor compression system integrated with enhanced phase change material. *Applied Thermal Engineering*, *182*, 116160. https://doi.org/10.1016/j.applthermaleng.2020.116160

Dhumane, R., Mallow, A., Qiao, Y., Gluesenkamp, K. R., Graham, S., Ling, J., & Radermacher, R. (2018). Enhancing the thermosiphon-driven discharge of a latent heat thermal storage system used in a personal cooling device. *International Journal of Refrigeration*, *88*, 599–613. https://doi.org/10.1016/j.ijrefrig.2018.02.005

Dittus, F. W., & Boelter, L. M. K. (1930). Heat transfer in automobile radiators of the tubular type. *University of California Publications in Engineering*, *12*(1), 3–22. https://doi.org/10.1016/0735-1933(85)90003-X

EnergyPlus™ (EnergyPlus™ (e+); 005462MLTPL00). (2017). National Renewable Energy Laboratory (NREL), Golden, CO (United States); Lawrence Berkeley National Laboratory (LBNL), Berkeley, CA (United States). https://www.osti.gov/biblio/1395882

Ermel, C., Bianchi, M. V. A., & Schneider, P. S. (2023). Energy Model to Evaluate Thermal Energy Storage Integrated with Air Source Heat Pumps: Preprint. *Renewable Energy*.

Fischer, D., Toral, T. R., Lindberg, K. B., Wille-Haussmann, B., & Madani, H. (2014). Investigation of Thermal Storage Operation Strategies with Heat Pumps in German Multi Family Houses. *Energy Procedia*, *58*, 137–144. https://doi.org/10.1016/j.egypro.2014.10.420

Focke, W. W., Zachariades, J., & Olivier, I. (1985). The effect of the corrugation inclination angle on the thermohydraulic performance of plate heat exchangers. *International Journal of Heat and Mass Transfer*, *28*(8), 1469–1479. https://doi.org/10.1016/0017-9310(85)90249-2

Hirschey, J., Gluesenkamp, K. R., Mallow, A., & Graham, S. (2018). Review of Inorganic Salt Hydrates with Phase Change Temperature in Range of 5 to 60°C and Material Cost Comparison with Common Waxes. *International High Performance Buildings Conference*. https://docs.lib.purdue.edu/ihpbc/320

Hong, K. T., & Webb, R. L. (1996). Calculation of Fin Efficiency for Wet and Dry Fins. *HVAC&R Research*, *2*(1), 27–41. https://doi.org/10.1080/10789669.1996.10391331

Huang, J., Fan, J., & Furbo, S. (2020). Demonstration and optimization of a solar district heating system with ground source heat pumps. *Solar Energy*, *202*, 171–189. https://doi.org/10.1016/j.solener.2020.03.097

Modelica/ModelicaStandardLibrary. (2024). [Modelica]. Modelica Association. https://github.com/modelica/ModelicaStandardLibrary (Original work published 2013)

Qiao, H., Aute, V., & Radermacher, R. (2015). Transient modeling of a flash tank vapor injection heat pump system – Part I: Model development. *International Journal of Refrigeration*, *49*, 169–182. https://doi.org/10.1016/j.ijrefrig.2014.06.019

Said, M. A., & Hassan, H. (2018). Parametric study on the effect of using cold thermal storage energy of phase change material on the performance of air-conditioning unit. *Applied Energy*, *230*, 1380–1402. https://doi.org/10.1016/j.apenergy.2018.09.048

SCE. (2023). *Business Time-Of-Use Rate Plans | Rates | Your Business | Home—SCE*. https://www.sce.com/business/rates/time-of-use

Shah, M. M. (2017). Unified correlation for heat transfer during boiling in plain mini/micro and conventional channels. *International Journal of Refrigeration*, *74*, 606–626. https://doi.org/10.1016/j.ijrefrig.2016.11.023

Shah, M. M. (2019). Improved correlation for heat transfer during condensation in conventional and mini/micro channels. *International Journal of Refrigeration*, *98*, 222–237. https://doi.org/10.1016/j.ijrefrig.2018.07.037

Shi, L., Liu, X., Qu, M., Liu, G., & Li, Z. (2021). Potential of Utilizing Thermal Energy Storage Integrated Ground Source Heat Pump System to Reshape Electricity Demand in the United States. *ASME Journal of Engineering for Sustainable Buildings and Cities*, *2*(031003). https://doi.org/10.1115/1.4051992

US. Dept. of Energy. (2024). Blueprint 2C: Building Efficiency & Electrification Campaign. *Energy.Gov*. https://www.energy.gov/scep/blueprint-2c-building-efficiency-electrification-campaign

Wetter, M., Zuo, W., Nouidui, T. S., & Pang, X. (2014). Modelica Buildings library. *Journal of Building Performance Simulation*, *7*(4), 253–270. https://doi.org/10.1080/19401493.2013.765506

Wilcox, S., & Marion, W. (2008). *Users Manual for TMY3 Data Sets (Revised)* (NREL/TP-581-43156). National Renewable Energy Lab. (NREL), Golden, CO (United States). https://doi.org/10.2172/928611

Yan, Y.-Y., Lio, H.-C., & Lin, T.-F. (1999). Condensation heat transfer and pressure drop of refrigerant R-134a in a plate heat exchanger. *International Journal of Heat and Mass Transfer*, *42*(6), 993–1006. https://doi.org/10.1016/S0017-9310(98)00217-8

ACKNOWLEDGEMENT

This material is based upon work supported by the U.S. Department of Energy's Office of Energy Efficiency and Renewable Energy (EERE) under the Building Technologies Office (BTO) Award Number DE-EE0009681. The views expressed herein do not necessarily represent the views of the U.S. Department of Energy or the United States Government. This work was also supported in part by the Modeling & Optimization Consortium at the Center for Environmental Energy Engineering at the University of Maryland.